Nanoscale

Accepted Manuscript

This article can be cited before page numbers have been issued, to do this please use: S. Chen, E. Olson, S. Jiang and X. Yong, *Nanoscale*, 2020, DOI: 10.1039/D0NR01740J.

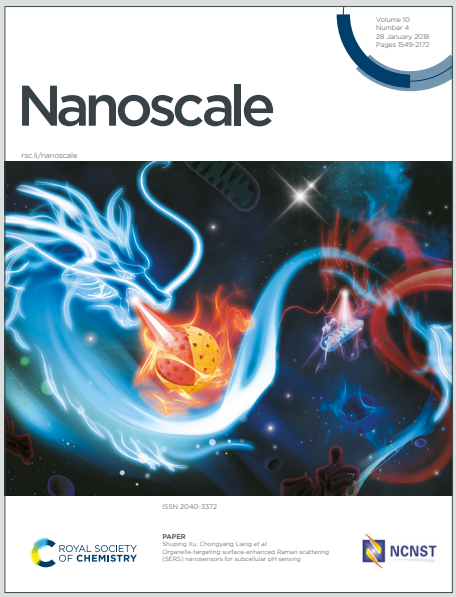

ROYAL SOCIETY OF CHEMISTRY

rsc.li/nanoscale

View Article Online
DOI: 10.1039/D0NR01740J

Nanoparticle assembly modulated by polymer chain conformation in composite materials

Shensheng Chen[a], Emily Olson[b], Shan Jiang[b†], Xin Yong[a*]
[a] Department of Mechanical Engineering, Binghamton University, Binghamton, New York 13902, USA
[b] Department of Materials Science and Engineering, Iowa State University of Science and Technology, Ames, IA 50011, USA

Abstract

Mixing nanoparticles into a strategically selected polymer matrix yields nanocomposites with well-controlled microstructures and unique properties and functions. The modulation of nanoparticle assembly by polymer chain conformation can play a dominant role in determining nanocomposite structures, yet such a physical mechanism remains largely unexplored. We hypothesize that highly ordered microdomains of rigid linear polymers provide a template for nanoparticle assembly into open fractal structures. We conducted mesoscopic computer simulations and physical experiments to elucidate how polymer chain conformation regulates dynamic evolution of nanoparticle structures during the drying processing of polymer nanocomposite films. The evaporation of polymer-nanoparticle mixtures with varying chain stiffness was simulated using dissipative particle dynamics. The formation of distinguished nanoparticle assemblies as a result of matrix selection was further corroborated by probing nanoparticle aggregation in different polymer nanocomposite coatings. The results show that polymer conformation not only influences the dispersion states of individual particles (dispersed vs. aggregated), but also modulates the morphologies of large-scale assembly (globular vs. fractal). The emergence of nematically ordered polymer clusters when the chain rigidity is increased creates local solvent-rich "voids" that promote anisotropic particle aggregates, which then percolate into open fractal structures upon solvent evaporation. The nanoparticle dynamics also exhibits an intriguing non-monotonic behavior attributed to the transitions between the coupling and decoupling with polymer dynamics. The nanoparticle assembly morphologies obtained in simulations match well with the electron microscopy images taken in physical experiments.

*Email: xyong@binghamton.edu

†Email: sjiang1@iastate.edu

View Article Online
DOI: 10.1039/D0NR01740J

Introduction

Polymer nanocomposites, a mixture of polymers or copolymers with nanosized particulates, offer remarkable improvements in mechanical, optical, thermal, and electrical properties compared to traditional polymeric materials.[1–4] Polymer nanocomposite materials acquire novel functions from nanoparticles while preserving useful properties of polymer. These materials exhibit low density, flexibility, and biocompatibility of the polymer matrix with enhanced functionalities provided by nanoparticles. This provides a broad range of applications in biomedicine, environmental sustainability, and food packing.[5–8] It is known that the performance of these hybrid materials is tightly correlated with the structure of polymer-particle interactions. Conventionally, nanoparticles need to be well dispersed for obtaining favorable rheological properties and optical transparency,[9,10] while a percolated particle network is preferred for enhancing mechanical strength and thermal conductivity.[3,11] Controlling the dispersion state and microstructure of the polymer-nanoparticle mixture, albeit being extensively studied,[6,12] still presents a major challenge in industrial processing techniques (e.g., casting or spraying). The difficulties here are ascribed to the perplexing enthalpic and entropic interactions among polymer, nanoparticle, and solvent, the largely unknown effects of polymer local confinement, and nonequilibrium perturbations of solvent evaporation.[12]

The influences of the chemical reactions between polymers and nanoparticles on particle assembly structure, such as core-shell nanoparticles grafted with polymers at surface, have been extensively studied.[13–17] Investigation of physical mechanisms that determine the composite microstructure are mostly limited to the effects of nanoparticle size, concentration, and shape.[14,18,19] However, the physical properties of polymers (especially molecular architecture and chain conformation) and their impact on particulate distribution and assembly in the mixture is not well understood. The physical confinement provided by the ordered polymer microdomains can affect nanoparticle dynamics, allowing for the design of nanocomposite materials with controlled microstructure. Previous work shows that chain stiffness has a great impact on the interfacial adsorption layer around nanoparticles[20] and the diffusion behavior of individual particles in

View Article Online
DOI: 10.1039/D0NR01740J

the polymer matrix.[21,22] These findings focused on single nanoparticle are of great interest, as they indicate that polymer conformation may play a role in the regulation of large-scale nanoparticle assembly. Recently, Olson et al. observed a percolated, mesoscale particle assembly structure in a polymer nanocomposite film of 2-hydroxyethyl cellulose (HEC) and zinc oxide (ZnO) nanoparticles. Upon changing the polymer matrix to 2-hydroxyethyl starch (HES), nanoparticles instead form globular aggregates.[23] Since the HES and HEC have identical chemical composition, the difference in the ZnO assembly structure is attributed to different polymer architectures (i.e., chain conformation and persistence length) of HES and HEC.[23] This result provides evidence to the concept of nanoparticle assembly driven by polymer conformation. Notably, several studies report polymers can form liquid crystalline ordering in the solution state with increasing persistence length.[24–26] Methylcellulose (MC), another cellulose derivates widely used in nanocomposites, can self-assemble into long fibrils in solutions, and this fibrillar formation is related to the polymer chain stiffness.[27,28] These examples of collective ordering of polymers in solution highlight the limitations of considering chains as uniformly distributed coils, which is assumed in many theoretical models of polymer-nanoparticle assembly. In addition, the spatial inhomogeneity and anisotropic interactions introduced by the polymer ordering can generate local confinement that modulate the nanoparticle assembly kinetics. All of the previous studies strongly suggest that an understanding of the influence of chain conformation on the particle assembly is necessary for uncovering structure-property relationships in polymer nanocomposites.

The relative size ratio between nanoparticle and polymer is critical for particle-polymer interactions in nanocomposite systems. When the particle size is much larger than characteristic length scales of polymer, it is well known that the depletion interaction will lead to the aggregation of particles.[29–31] This behavior is entropy driven, in which the polymer chains maximize their entropy as the particles decrease their exposure to polymers by aggregation.[29,32] The depletion interaction diminishes as the particle size decreases to be comparable or smaller than the polymer coil size.[32,33] For direct comparison with the experimental results, the size of nanoparticles in the simulation study is set to be comparable to the size of polymer coils. Therefore, depletion force is negligible.

View Article Online
DOI: 10.1039/D0NR01740J

In this work, we performed mesoscopic simulations to provide insights into the effects of polymer conformation on the dynamic evolution of nanoparticle assembly structure. The simulation couples the thermodynamic equilibrium of bulk polymer-nanoparticle mixtures with explicit solvent evaporation to model the typical casting process of polymer nanocomposite films. The results discover that the dynamics and final assembly structure of nanoparticles are strongly dependent on the polymer conformation. In particular, the solvated polymers change their collective structure from being randomly distributed to highly ordered when the chain rigidity is increased. Surprisingly, the nanoparticle dynamics varies non-monotonically as polymer stiffness increases a result of their interaction with surrounding polymers. The particle diffusion is first suppressed but subsequently enhanced after long-range orientational order emerges. The ordered clusters of polymers create local "voids" that are free of polymers, in which nanoparticles are favorably dispersed. These polymer microdomains then promote the anisotropic assembly of nanoparticles during evaporation and ultimately guide the percolation of fractal structures in the dry composite. The chain-conformation-controlled mechanism of the nanocomposite microstructure evolution is corroborated with the experimental evidence in polymer nanocomposite films containing different nanoparticles including ZnO, titanium dioxide (TiO_2), and silica (SiO_2) nanoparticles in HEC and HES matrices. The results suggest that the drastic change in nanocomposite structures observed with different chain conformations may not depend on the specific chemistry of nanoparticles. This work not only reveals the physics of polymer-structure-modulated nanoparticle dynamics, but also provide a simple approach for engineering nanocomposite materials with desired structures.

Methods

We performed computational studies of polymer nanoparticle mixtures with cast solvent using dissipative particle dynamics (DPD).[34,35] DPD is a mesoscale method widely used in the simulations of complex fluid systems. In DPD, individual spherical, coarse-grained bead represents a group of small molecules. The dynamics of these beads is governed by Newton's second law. The total force on bead i is calculated from the pairwise forces between beads i and j. Each pairwise interaction contains three parts:

View Article Online
DOI: 10.1039/D0NR01740J

conservative force, dissipative force, and random force: $\mathbf{F}_i = \sum\left(\mathbf{F}_{ij}^{\mathrm{C}} + \mathbf{F}_{ij}^{\mathrm{D}} + \mathbf{F}_{ij}^{\mathrm{R}}\right)$. The sum runs over all beads within a certain cutoff radius r_{c} from bead i. The conservative part is given by $\mathbf{F}_{ij}^{\mathrm{C}} = a_{ij}(1-r_{ij})\mathbf{e}_{ij}$, where a_{ij} is the maximum repulsion between beads i and j; $r_{ij} = \left|\mathbf{r}_i - \mathbf{r}_j\right| / r_{\mathrm{c}}$ is the inter-bead distance; and $\mathbf{e}_{ij} = \left(\mathbf{r}_i - \mathbf{r}_j\right) / \left|\mathbf{r}_i - \mathbf{r}_j\right|$ represents the force direction. The interaction strength a_{ij} between the beads of the same species is set to 25. This value has been parametrized to recover the compressibility of water.[35] The miscibility of different fluid components is controlled by the excess repulsion, which is defined as the difference in repulsion between the dislike- and like-species repulsions. Compared with the Lennard-Jones potential used in molecular dynamics and Brownian dynamics, the soft-core linear force $\mathbf{F}_{ij}^{\mathrm{C}}$ permits the use of much larger time steps in DPD and thus allows simulations to access larger time and length scales.

The dissipative force $\mathbf{F}_{ij}^{\mathrm{D}}$ scales with the relative velocity of two beads $\mathbf{v}_{ij} = \mathbf{v}_i - \mathbf{v}_j$, given by $\mathbf{F}_{ij}^{\mathrm{D}} = -\gamma w_{\mathrm{D}}(r_{ij})(\mathbf{e}_{ij} \cdot \mathbf{v}_{ij})\mathbf{e}_{ij}$. The random force is given by $\mathbf{F}_{ij}^{\mathrm{R}} = \sigma w_{\mathrm{R}}(r_{ij})\xi_{ij}\mathbf{e}_{ij}$, where ξ_{ij} is a random variable with Gaussian statistics $\langle\xi_{ij}(t)\rangle = 0$ and $\langle\xi_{ij}(t)\xi_{i'j'}(t')\rangle = (\delta_{ii'}\delta_{jj'} + \delta_{ij'}\delta_{ji'})\delta(t-t')$. w_{D} and w_{R} are arbitrary weight functions depending on the interparticle distance; γ determines the strength of viscous dissipation; and σ is the noise amplitude. The magnitudes of the dissipative and random forces are correlated with each other through the fluctuation-dissipation theorem.[35] The theorem requires $\left[w_{\mathrm{R}}\left(r_{ij}\right)\right]^2 = w_{\mathrm{D}}\left(r_{ij}\right) = \left(1-r_{ij}\right)^2$ and $\sigma^2 = 2k_{\mathrm{B}}T\gamma$, with k_{B} being the Boltzmann constant. This relation also determines the temperature of a DPD system T. As per convention, DPD simulations consider all beads having the same mass m. The cutoff radius r_{c} and energy of thermal fluctuation $k_{\mathrm{B}}T$ are selected as the characteristic length and energy scales, respectively. Based on the dimensional analysis, the characteristic time for DPD is thus given as $\tau = \sqrt{mr_{\mathrm{c}}^2 / k_{\mathrm{B}}T}$. We present the simulation results in reduced units with r_{c}, m, and $k_{\mathrm{B}}T$ all set to one, which also give $\tau = 1$.

View Article Online
DOI: 10.1039/D0NR01740J

Unless stated otherwise, polymers are simulated as monodisperse chains using the simple bead-spring model. Individual chain is constructed by a sequence of $N_p = 150$ DPD beads connected with harmonic bonds. As a result, the polymer beads experience additional permanent bond force $\mathbf{F}_{ij}^{B} = -B(r_{ij} - b)\mathbf{e}_{ij}$ with a spring constant $B = 128$ and an equilibrium bond length $b = 0.5$. In order to control the chain stiffness and conformation, a bending potential given by $E = K\left[1 + \cos(\theta)\right]$ is incorporated.[36–38] The parameter K tunes the strength of the potential and stiffness of the chains. For a chain with $K >= 2$, the stiffness parameter is related to the persistence length via $l_p \approx bK$.[22,37] In this work, we systematically change K from 2 to 50 to control the polymer conformation and investigate its influence on the polymer-nanoparticle assembly. To represent more realistic polymer architecture (e.g., HEC), We also simulated the stiff polymers with side chains that have different weight fractions to the backbone. Notably, the parameters of bead-spring model in DPD need to be carefully selected. Soft conservative forces between DPD beads allow bond crossing and topological violation of polymer chains. These simulation artifacts can lead to unrealistic chain dynamics if occur frequently, especially in dense and entangled polymeric systems.[39–41] Improved models such as the multi chain approach[40] and segmental repulsive potentials[42] have been developed to address this issue but they substantially increase computational costs. On the other hand, the unphysical bond crossing in DPD can also be largely reduced by selecting appropriate bond and angle potentials for the polymer model.[43] Other studies have shown that stiff and short harmonic bonds with the addition of angle potentials effectively suppress bond crossing and allow DPD simulations to capture polymer dynamics correctly.[44–46] We select similar parameters for the polymer model used in this work.

Each nanoparticle is constructed from a face-centered cubic (FCC) cluster of DPD beads that is truncated into a spherical shape. An additional layer of DPD beads is introduced to impose a well-defined particle surface with a high degree of symmetry.[47,48] The number density of constituent beads in nanoparticles is set to 10 to prevent unphysical overlapping among nanoparticles, polymers, and solvent.

View Article Online
DOI: 10.1039/D0NR01740J

The particles have a radius of 1 and move as rigid bodies. Thus, the nanoparticles are comparably smaller than the softest polymer coil which has a radius of gyration of 8 measured at $K = 2$. This size difference eliminates the depletion effect prevalently considered in polymer nanocomposite systems. To represent the chemistry of many inorganic nanoparticles such as ZnO,[12,23] the modeled nanoparticles are set to be well dispersed in aqueous solvent but enthalpically incompatible with polymers. To model miscibility and immiscibility between different components, DPD interaction parameters across differing types of beads are set based on our previous results.[49,50] Namely, the incompatibility between the nanoparticle and polymer is controlled by setting the DPD repulsion parameter $a_{\mathrm{NP}} = 35$, where N, P represent bead types of nanoparticles and polymers, respectively. The rest of the repulsion parameters are set to $a_{ij} = 25$. We consider polymer nanocomposite mixtures with 50% water content as the initial polymer solution samples before evaporation. The weight ratio between the polymers and nanoparticles is set to 9:1. The total numbers of polymer chains and nanoparticles are 639, and 217, respectively.

All simulations are initially conducted in cubic domains of dimensions $40\times40\times40$ or $100\times100\times100$ with periodic boundary conditions applied in all directions. The total number density is set to 3 per convention for DPD.[35] The time step is $\Delta t = 0.005$ and an equilibrium simulation typically runs 3,000,000 time steps for probing the microstructure evolution. For probing nanoparticle dynamics, longer simulations of 10,000,000 time steps are conducted for calculating the mean squared displacement and diffusivity of particles. An evaporation simulation is conducted after the equilibrium to investigate the final nanoparticle assembly. The characteristic time scales of physical evaporation in experiments are orders of magnitude larger than the time scales of structural development on the particle and chain level. Modeling continuous evaporation while resolving the detailed dynamics of polymer and nanoparticles is beyond the accessible computational time. Thus, we exploit a stepwise approach to gradually decrease the water content in the bulk to mimic the evaporation process. In short, after equilibrium, we remove 25% of water beads and let the simulation run 400,000 timesteps for reaching new equilibrium. This process repeats until all water beads are evaporated out. To keep the total number density as a constant, the simulation domain

View Article Online
DOI: 10.1039/D0NR01740J

shrinks isotopically every time of solvent evaporation.

Physical experimental procedure of forming the nanocomposites are detailed in the electronic supplementary information.

View Article Online
DOI: 10.1039/D0NR01740J

Results and Discussion

A. Equilibrium with solvent

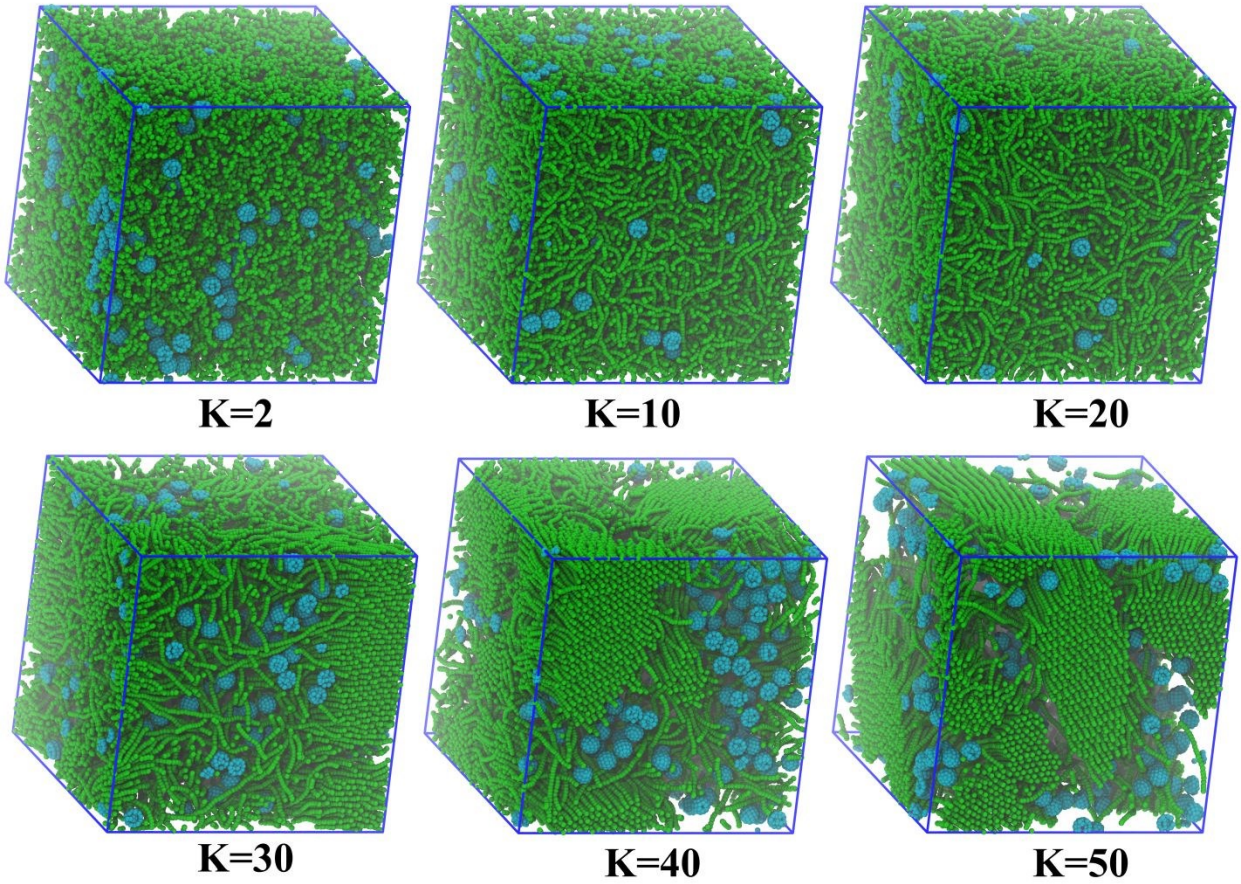

Figure 1. Final polymer-particle morphologies for equilibrium runs under the solvation of 50% water, with polymer stiffness parameter K = 2, 10, 20, 30, 40, and 50 respectively. The green beads represent polymer beads, the cyan beads represent particle beads. Water beads are not displayed for clarity.

Figure 1 shows that the polymers form ordered and compact structures at equilibrium as the chain stiffness increases. The polymers clearly assemble into locally nematic bundles with stiffness parameter $K >= 30$. The bundling of long-persistence-length polymers in solution agrees well with previous theoretical and experimental findings.[24,25,27,51–56] The formation of the ordered polymer domains is driven

View Article Online
DOI: 10.1039/D0NR01740J

by the reduction of significant bending energy when stiff polymers align.[53,57] The kinetics of this microphase separation is describable by a nucleation and growth mechanism.[57] In particular, the collective bundling of polymer chains dominates the kinetics by increasing the energy barrier for entropy-driven rearrangements of the chains.[54,57,58] The ordering of rigid polymer may be augmented by the intramolecular hydrogen bonds as in native cellulose.[59] We calculate the nematic order parameter of the polymer backbone $S = \left\langle \left(3\cos^2\theta_{ij} - 1\right)/2 \right\rangle_{i \neq j}$ to quantitatively characterize the local orientational ordering of polymer in the equilibrium simulations.[51,52] Here, θ_{ij} is the angle between two bond vectors *i* and *j*, $\langle \rangle$ represents spatial average of all pairs of bond vectors within a cutoff distance of $5r_c$. We stress that changing the cutoff distance does affect the absolute values of nematic order parameter but has no influence on its relative behavior for different *K*. Figure 2 clearly shows *S* increases as *K* increases. Especially, when $K >= 30$, the time evolution of nematic order shows the polymers gradually develop orientational order during equilibrium. While *K* is less or equal to 20, these relatively soft polymers relax to homogenous structures with no sign of bundling. Interestingly, coexistent with highly ordered polymer structures (e.g., $K = 40$ and $K = 50$ in Figure 1) the nanoparticles are localized in the solvent-rich regions created by the bundling of polymers. These rigidity-induced self-organization of polymer has a clear influence on the nanoparticle dynamics and assembly. Videos S1-S3 present complete time evolution of polymer-nanoparticle mixtures for several representative K values.

View Article Online
DOI: 10.1039/D0NR01740J

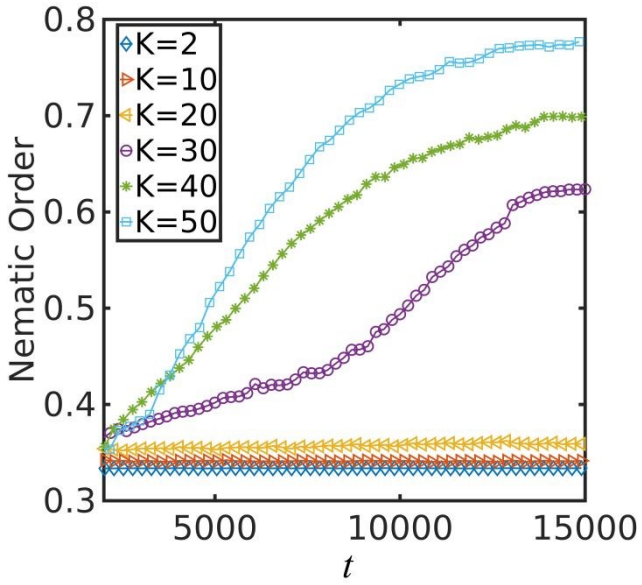

Figure 2. Polymer nematic order parameters during the equilibrium runs for different polymer stiffness.

The mean squared displacements (MSD) of nanoparticles $\left\langle \Delta r^2 \right\rangle = (1/N)\sum_{i=1}^{N}\left\langle \left[r_i^{\mathrm{com}}(t) - r_i^{\mathrm{com}}(0) \right]^2 \right\rangle$ are calculated to elucidate the detailed dynamics of the nanoparticles, which are important for microstructure evolution. Here, N is the total number of nanoparticles. $r_i^{\mathrm{com}}(t)$ is the position of the center of mass a particle at time t. The dynamics of nanoparticles can be inferred by the relation $\left\langle \Delta r^2 \right\rangle \sim t^{\upsilon}$ with υ being an exponential fitting constant. Figure 3(a) shows the MSD profiles for different K at equilibrium. Interestingly, the nanoparticle dynamics exhibits diffusive scaling with $\upsilon \approx 1$ on long time scales ($t > 10^4$) in all systems despite distinct polymer structures observed in Figure 1. A sub-diffusive region can be observed on short time scales ($10^2 < t < 10^3$) as polymer stiffness increases. This short-time subdiffusion is attributed to the increased coupling between nanoparticles and the segmental relaxations of the surrounding polymer chains.[22,60,61] However, the subdiffusive behavior disappears when the microphase separation between highly rigid polymers and solvent occurs, suggesting the long-time normal diffusion

View Article Online
DOI: 10.1039/D0NR01740J

220 observed in both the homogeneous systems with flexible polymers and the partitioned systems with rigid
221 polymers have rather different underlying dynamics.

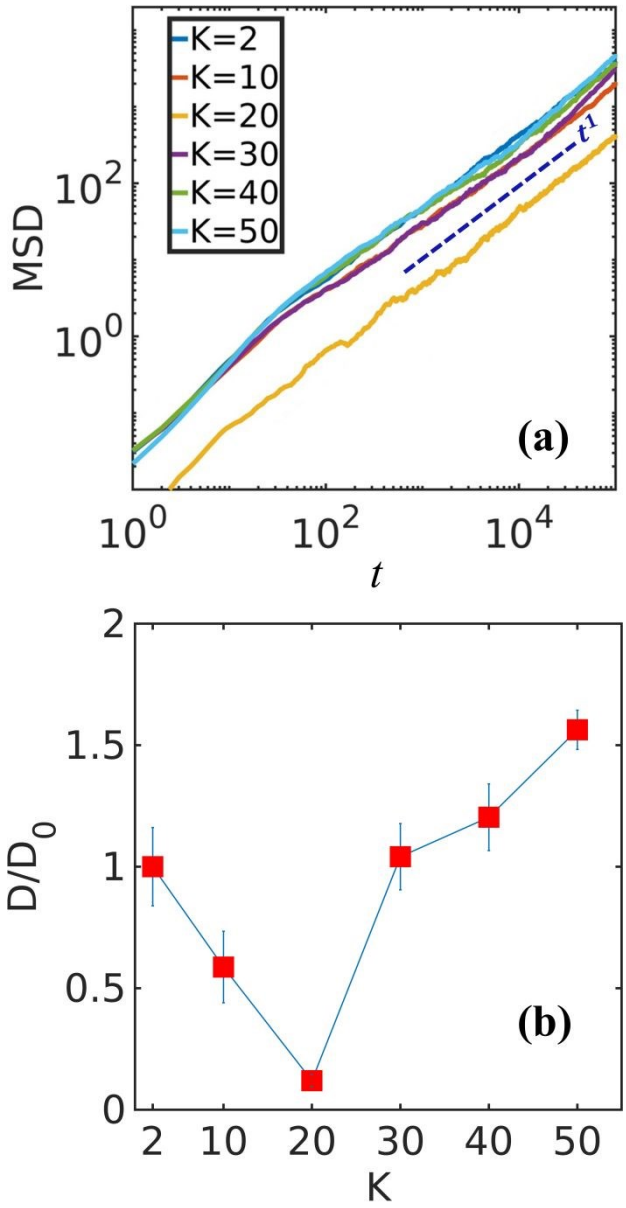

222

223 Figure 3. (a) The mean squared displacements of particles in the long-time equilibrium runs for different
224 polymer stiffnesses. (b) Normalized particle diffusivity D / D_0 of equilibrium runs for K = 2, 10, 20, 30,
225 40, and 50, respectively. Where D_0 represents the diffusivity for K = 2. The error bars represent the
226 standard deviations among 5 measured segments in the diffusive regions of the MSD.

View Article Online
DOI: 10.1039/D0NR01740J

To uncover more details in the long-time diffusion of nanoparticles, we calculate nanoparticle diffusivity D by fitting the diffusive region of the MSD curve to $\left\langle \Delta r^2 \right\rangle = 6Dt$. As shown in Figure 3(b), the diffusivity changes nonmonotonically as the polymers become stiffer. In particular, the diffusivity first decreases as polymer stiffness increases to $K = 20$ while the mixture remains homogeneous. The long-time diffusion in homogeneous and dense polymer solutions and the diffusivity decrease can be described by the mode-coupling theory.[22,62,63] Surprisingly, the diffusion of nanoparticles is significantly enhanced with increasing chain stiffness when $K \geq 30$. The value of the diffusivity even exceeds the one in the system with the most flexible polymers ($K = 2$) and increases as K further increases. This enhanced diffusion is induced by the polymer-solvent phase separation. As the polymer nematic ordering develops, the nanoparticles concomitantly migrate to the solvent-rich regions. Particles dispersed in the background solvent are shown to decouple from typical polymer dynamics. We expect the diffusivity to obey the Stoke-Einstein relation. Besides influencing the nanoparticle dynamics, the boundaries and the connections of the "openings" in the polymer matrix introduce physical confinement for large-scale nanoparticle assembly. We speculate that as solvent evaporates, these "openings" will "mold" the nanoparticle aggregates into an open fractal structure.

B. Evaporation

After equilibrium, evaporation is modeled by stepwise removal of 25% of the total initial solvent beads. Figure 4(a) shows the snapshots of the system of $K = 50$ at solvent evaporation percentages of 0%, 25%, 50%, 75%, and 100%, respectively. The nanoparticles are initially dispersed in the "voids" without notable agglomeration. In the final stage, the nanoparticles are caged by the boundaries of polymer bundles. Figure 4(b) displays the final particle assemble structure after evaporation for different values of K. It is clearly shown that the nanoparticles assemble into large clusters at low ($K = 2$) and high ($K = 40$ and 50) polymer stiffness. Notably, at intermediate stiffnesses, the nanoparticles are relatively dispersed. The

View Article Online
DOI: 10.1039/D0NR01740J

simulations also uncover that the clusters formed in the soft polymer matrix resemble globular aggregates, while the assembly in rigid polymer matrix is clearly more anisotropic. The distinct aggregation morphologies at low and high polymer stiffness and the dispersive particle distribution at intermediate polymer stiffness confirms the significant impact of polymer conformation on the large-scale nanoparticle assembly. Videos S4-S6 show the detailed evolution of the systems under evaporation for different K.

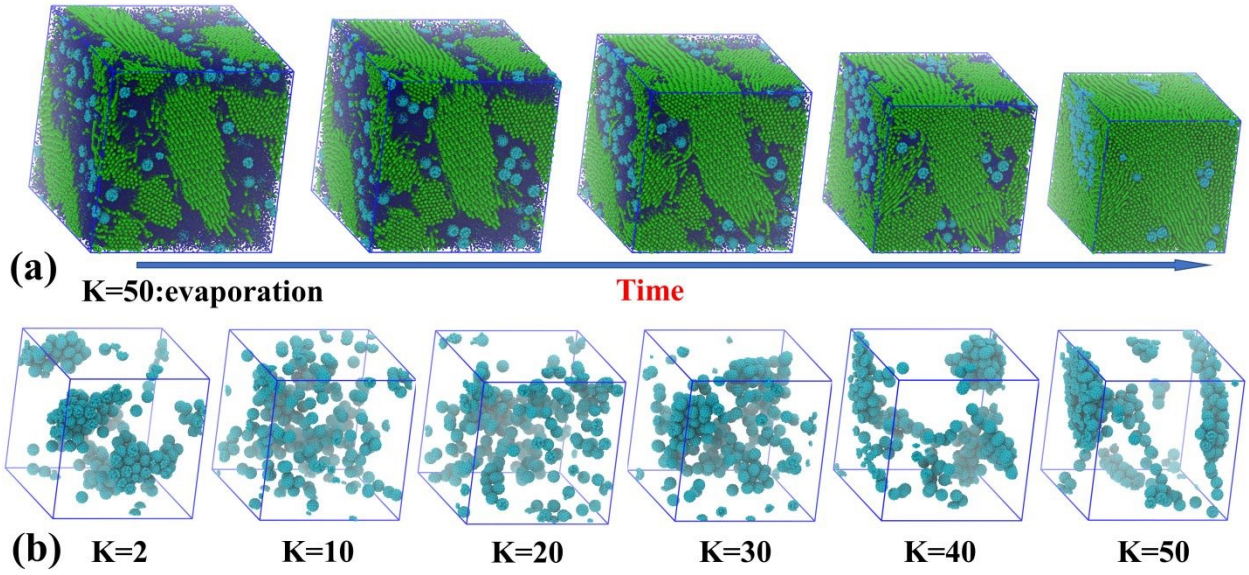

Figure 4. (a) Time evolution morphologies during evaporation runs for K = 50. The blue regions are filled with water beads. (b) Final particle morphologies of particles after evaporation for K = 2, 10, 20, 30, 40, and 50, respectively.

The MSD plotted in Figure 5 quantifies the detail particle dynamics during evaporation in the systems of different polymer conformations. The reducing slope of MSD indicates that the dynamics of particles become slower and slower as water evaporates. The plateaus in the MSD curves show that the nanoparticles are gelated at the end of evaporation in all the simulations expect for the softest polymer system ($K = 2$). The nanoparticle dynamics in evaporation shows similar behavior as during equilibrium: the particles move slower in the polymers with intermediate stiffness and much faster in low and high stiffness systems. This means that the polymer structures resulting from different chain stiffness and

View Article Online
DOI: 10.1039/D0NR01740J

conformation is maintained during evaporation.

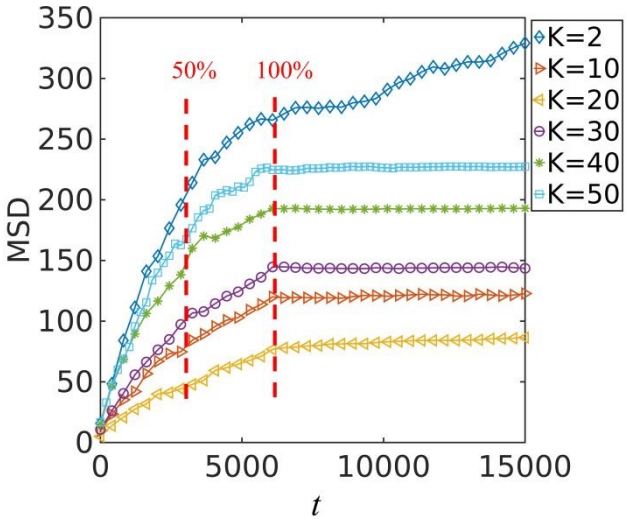

Figure 5. Mean square distance of particles for K = 2, 10, 20, 30, 40, and 50 during evaporations. The dash lines mark the progression of solvent evaporation.

We calculate the particle connectivity and cluster anisotropy to quantify the assembly structure. We define connected particles of radius r when their center-to-center distance is less than d_r, where $d_r = 2r + \delta$ with $\delta = 0.1r$ as a tolerance introduced for reducing the effect of thermal fluctuations in the cluster clarification. A cluster of particles is formed when there are more than N_{cf} particles being linked together. We select $N_{\mathrm{cf}} = 12$ as it is the maximum nearest neighbor number of one particle. The degree of particle connectivity is given by $N_{\mathrm{c}}/N_{\mathrm{total}}$, where N_{c} is the total number of particles that form clusters and N_{total} is the total number of particles. The average cluster anisotropy of the polymer nanocomposite is given by $\sum_i w_i a_i$, where $w_i = N_i / N_{\mathrm{c}}$ and a_i are the weight fraction and relative shape anisotropy[64] of cluster i.

As shown in Figure 6, the particle connectivity is lowest for polymer stiffness $K = 20$, indicating

View Article Online
DOI: 10.1039/D0NR01740J

a more dispersed particle distribution. The high values of connectivity for both softer and stiffer polymer systems confirm that the high degree of nanoparticle aggregations observed in the simulation snapshots. The low cluster anisotropy value of soft polymers ($K = 2$) corresponds to the globular clusters. When the polymers are stiff enough to form bundling structures ($K > 30$), the cluster anisotropy clearly increases, suggesting the high possibility of forming an open fractal network. The more spherical clusters formed in the soft polymer matrix is thermodynamically driven, as a result of the minimization of unfavorable enthalpic interactions between polymers and nanoparticles. The more dispersed state of particles in the intermediate stiffness polymer system is attributed to the homogenous increase of viscous hindrance within the entire bulk phase, which uniformly inhibits particle diffusion. While in the system with local polymer bundles, the formation of anisotropic particle clusters is physically driven. The "voids" in these systems not only offer extra space for particle aggregation, but also provide physical boundaries and connections for the aggregates. Thus, the polymer conformational characteristic not only influences the dispersion state of particles (dispersed vs. aggregated), but also influence the structure of particle assembly (globular vs. fractal). This resembles what has been observed in the experiments of ZnO-laden polymer films.[23]

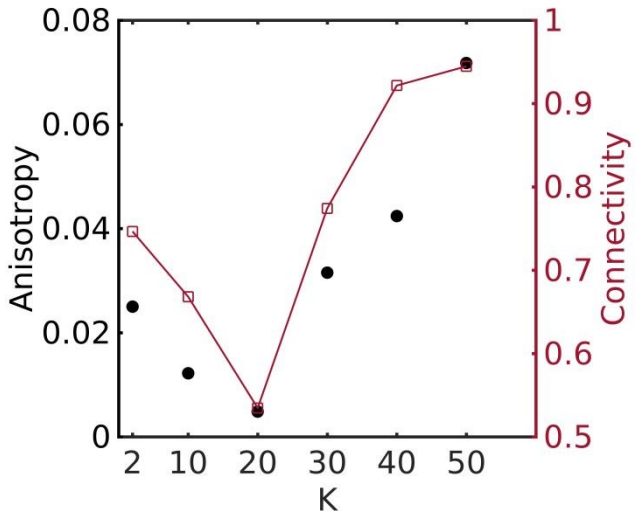

Figure 6. Particle anisotropy and connectivity at the end of evaporation for different polymer stiffness parameters *K*. The filled circle points are anisotropy values and the red plot shows the connectivity.

View Article Online
DOI: 10.1039/D0NR01740J

Figure 7 plots the time evolution of particle connectivity during evaporation for different polymer stiffnesses. Overall, the connectivity increases with the decrease in water content. Note that in soft polymer systems ($K = 2$), the particles form clusters gradually, which become stable before the end of evaporation. This confirms that the particles diffuse faster and can rapidly aggregate in flexible polymer matrices. Interesting, the connectivity at the early stage of the high stiffness systems ($K = 40$ and 50) is almost zero, which indicates that the nanoparticles are initially well dispersed in the polymer-free "void" regions induced by the bundling of polymers. As evaporation reaches its late stage, the connectivity exhibits a significant increase. In the $K = 50$ system, the connectivity exhibits a nearly first-order jump. These variations in connectivity in high stiffness polymer systems confirm our hypothesis that the particles are confined in the "voids" between ordered polymer microdomains during evaporation. As water being evaporated out, particle aggregation happens as a result of the compression of the boundaries of polymer bundles. In order words, these polymer structure molds the final nanoparticle assembly.

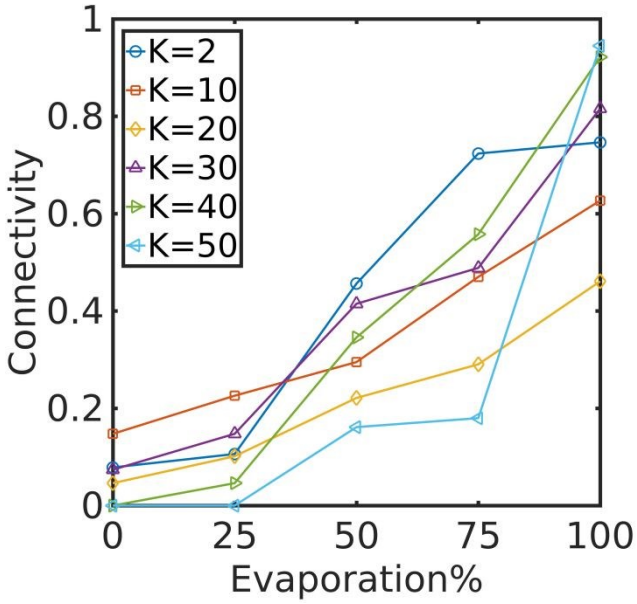

Figure 7. Particle connectivity during evaporation for different polymer stiffness systems. The horizontal axis represents the percentage of water being evaporated.

View Article Online
DOI: 10.1039/D0NR01740J

C. Side chain effect

As demonstrated above, the anisotropic particle cluster formation in high polymer stiffness systems relies on the development of polymer nematic bundles, which creates local "cracks" that influence the dynamics of the particles. In many physical systems of polymer nanocomposites, the molecular architectures of polymer are more complicated than the simple "backbone" model. Polymers usually have side chain groups added to the backbone, and these side chain may disrupt the polymer assembly ordering. In order to further demonstrate the importance of polymer crystallization on the nanoparticle assembly, as well as to represent more realistic polymer architectures, we incorporate soft side chains into to the backbones of stiff polymers ($K = 50$) and perform the same simulations as before to study its influence. The side chain concentration varies from 0% to 40%. Each side chain is modeled as a soft chain ($K = 2$) by connected N_s DPD beads, where N_s is randomly drawn from a normal distribution with a mean of 10 and a standard deviation of 1. The side chains are grafted to random positions along the backbone.

The snapshots in Figure 8(a) shows the polymer structure with orientational ordering at the end of equilibrium is greatly disturbed by increasing the concentration of side chain. When the side chain concentration is larger than 20%, the bundling completely diminishes. The weakening of the liquid crystalline ordering by adding soft side chains is further confirmed by the polymer nematic order parameter in Figure 8(c), in which the nematic order parameter is greatly reduced as the side chain concentration increases. This change in the polymer nematic ordering then influences the particle assembly. After evaporation, the final particle anisotropy and connectivity in Figure 8(d) also confirms that the particle assembly gradually loses anisotropy and becomes relatively random dispersion. These control simulations further confirm that the key to forming particle fractal cluster is the "cracks" induced by the ordering of polymers. Notably, in physical systems like cellulose derivatives, increasing the side chain length and the degree of substitution decrease the degree of crystallinity but do not completely remove the crystalline domain.[65–68] The detailed dynamics of the systems with different side chain concentrations can be seen in

View Article Online
DOI: 10.1039/D0NR01740J

341 Videos S7-S10.

342

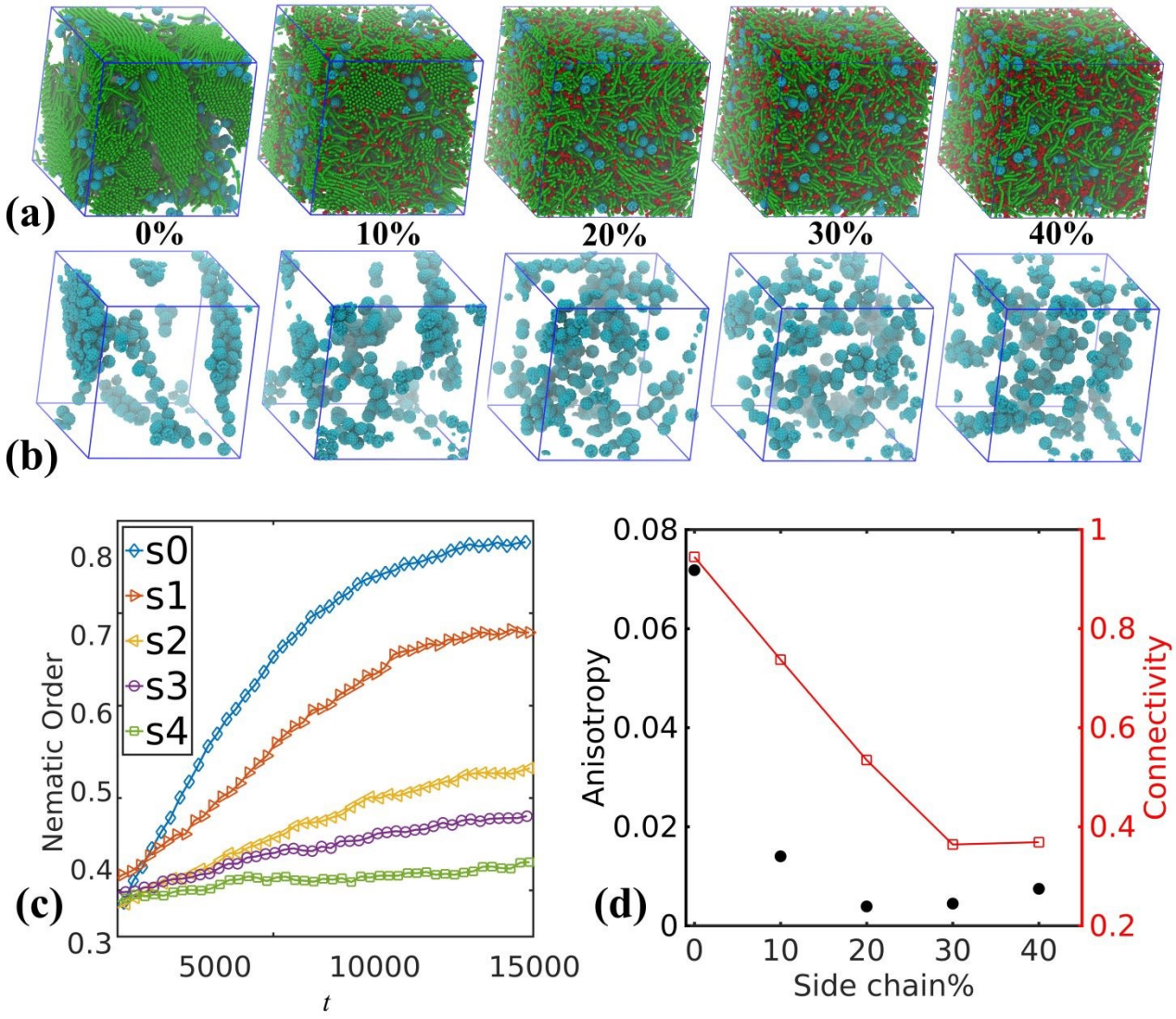

343

344 Figure 8. (a) Final polymer-particle morphologies for equilibrium runs under the solvation of 50% water at
345 K = 50, with soft side chain polymer fractions of 0%, 10%, 20%, 30%, and 40%, respectively. The red
346 beads are side chain beads. (b) The corresponding final morphologies of particle assembly after complete
347 evaporation. (c)The nematic order parameters of the polymer backbone during the equilibrium runs for
348 systems with different fractions of side chain beads. (d) Particle anisotropy and connectivity at the end of

View Article Online
DOI: 10.1039/D0NR01740J

evaporation for systems of different side chain percentages. The filled black circles are anisotropy values and the open red squares show the connectivity.

D. Experiments of nanoparticle structures in HEC and HES matrices

Central to the distinct nanoparticle aggregate formation observed in our simulations is the difference in the conformations of polymer chains. We further conducted experiments on polymer nanocomposites to probe the nanoparticle assembly structures in physical systems. Our model systems had HEC and HES as the coating matrices with various types of nanoparticles embedded within. Figure 9(a) displays similar fractal aggregation structures of different nanoparticles assembled in the HEC matrix, which are consistent with the structure observed in the large-scale simulation with stiff polymer (K = 50) shown in Figure 9(b). In contrast, dense globular clusters of particles were formed in the HES coatings and the K = 2 simulation system. The similar transition for different nanoparticles from globular clusters to fractal aggregation structures when polymer matrix is switched from HES to HEC suggests that the change may be a result of physical effects, instead of the specific interactions between nanoparticle and polymer matrix. Prior studies indicate that the persistence length of HEC is significantly longer than that of HES.[69,70] These experimental findings show good qualitative agreement with the simulation results with varying polymer stiffness, and confirm our findings of the important role of polymer conformational characteristics on the morphological assembly of nanoparticles.

These new results highlight that our understanding of nanoparticle structure formation in polymer nanocomposites is still incomplete. This study serves the starting point of our efforts in uncovering mechanisms that govern nanoparticle assembly in different polymer matrices. The mesoscopic simulation represents a model system in which not all interactions relevant in experiment are considered explicitly. For example, long-range electrostatic interactions are important for colloidal assembly in polymer

View Article Online
DOI: 10.1039/D0NR01740J

nanocomposites,[71,72] but have not been considered here. Numerical methods for incorporating electrostatic interactions in DPD have been developed by multiple groups including us,[73,73–76] and are readily available for future studies of electrostatic effects in this system. Other specific interactions such as hydrogen bonding[77,78] are dependent on surface chemistry of nanoparticles, which can be studied implicitly in our simulations by varying the effective interactions between components. Notably, increasing chain rigidity has been shown to increase the interfacial adsorption layer thickness in polymer nanocomposites.[20] This enhanced adsorption of rigid polymers could promote the interparticle attractions mediated by the interfacial layers and lead to the fractal aggregation. The interfacial properties of polymer nanocomposites and the possible bridging effect on the nanoparticle assembly could be significantly affected by the size of nanoparticles,[79–81] which will be investigated in future work.

View Article Online
DOI: 10.1039/D0NR01740J

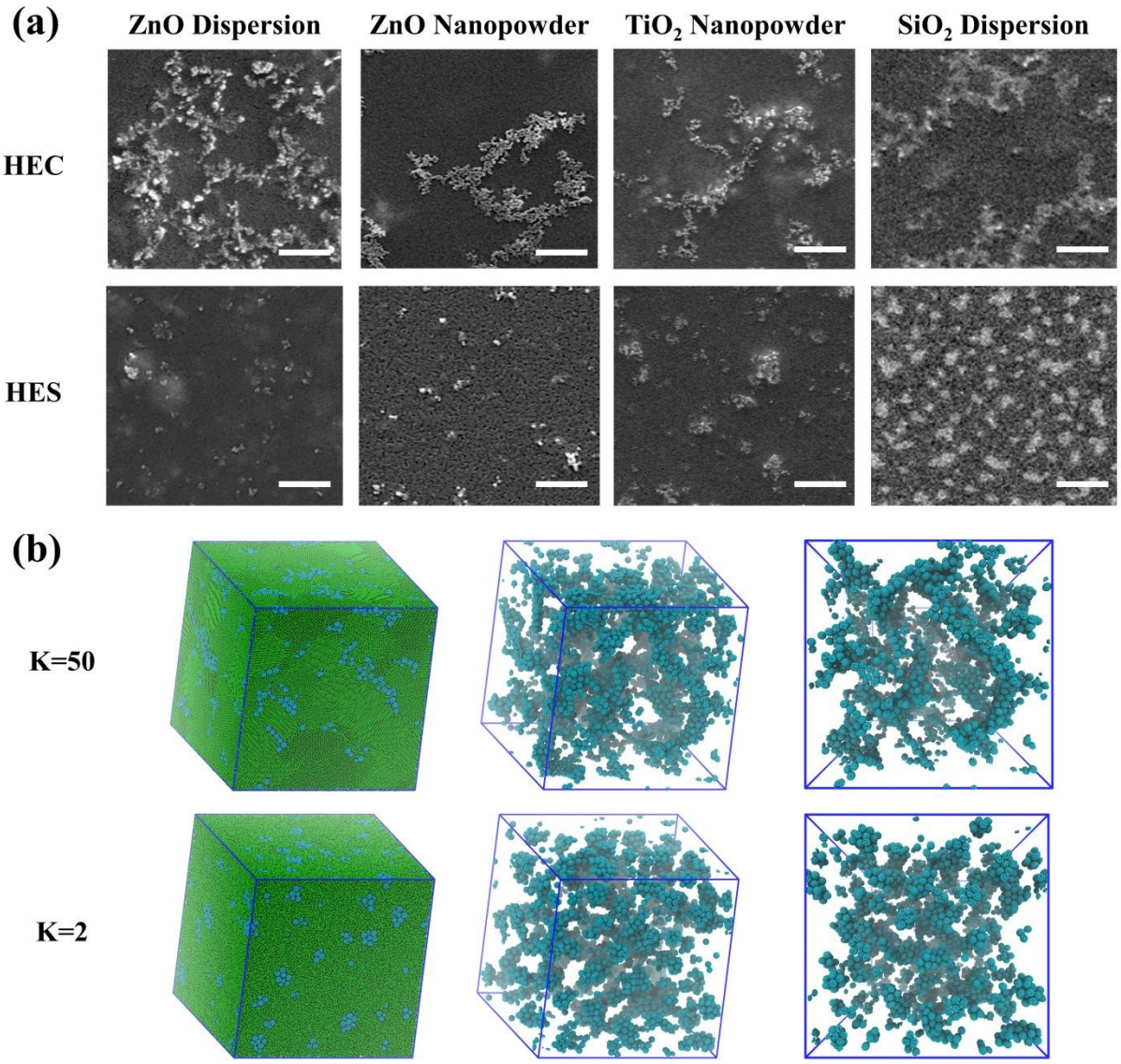

Figure 9. (a) Scanning electron microscopy micrographs of the nanoparticle aggregation patterns in dried coating films in hydroxyethyl cellulose (HEC) and hydroxyethyl starch (HES) polymer binders. These nanoparticles demonstrate similar assembly behaviors as a result of matrix selection. All nanoparticles are of 20-50 nm in diameter. The labels in the figure indicate the original format of the commercially acquired nanoparticles. Scale bar is 1 μm. (b) Snapshots of dried polymer nanocomposites and nanoparticle structures at different viewing angles obtained in the large-scale ($100\times100\times100$) simulations. The results show the percolation of anisotropic aggregates into open fractal structures in the rigid polymer matrix in contrast to the globular clusters in the soft polymer matrix, consistent with experiments.

View Article Online
DOI: 10.1039/D0NR01740J

Conclusions

In summary, this study highlights the importance of polymer conformation on the modulation of the nanoparticle assembly via particle thermodynamics, kinetics, and imposing physical confinements. The simulation results show that polymers form highly ordered microdomains in solution as the persistence length increases. These polymer structures in turn have a great impact on the dynamics and assembly of the nanoparticles. The final nanoparticle assembly shows a clustered-dispersed-clustered structural transition with increasing polymer stiffness. In very soft polymer systems, the nanoparticles form globular aggregates driven by unfavorable polymer-nanoparticle interactions. In intermediate stiff polymer systems, the nanoparticles are well dispersed as particles kinetics being arrested in the polymer matrix. When polymer stiffness is high, the nanoparticles assemble into anisotropic clusters in the polymer-free "cracks" formed concurrently with the local crystallization of the rigid polymers. The critical role of the "cracks" on the formation of mesoscale fractal particle structures is further elucidated in the comparative study of the stiff polymer systems with side chains. The important role of polymer conformation on the morphological assembly of nanoparticles was further corroborated by the experiments observing assembly structures of different types of nanoparticles in the polymer matrices with different chain architectures.

Our simulation and experimental results suggest one can readily leverage chain conformation to simultaneously modulate the polymer and nanoparticle assembly structures in polymer nanocomposites. In particular, the local crystallization of stiff polymer bundles inhibits isotropic nanoparticle aggregation and results in the formation of percolated particle networks. This fractal particle structure can play important roles in a wide range of thin film applications. Moreover, polymers with specific molecular architectures (e.g., block copolymers) can be programmed to yield more complex structures for physically guiding local nanoparticle aggregations into a well-defined, large-scale assembly. Unique properties can emerge in polymer nanocomposites by controlling the particle assembly structure that spans different length scales. The findings provide new ideas and opportunities for innovating design principles of structural

View Article Online
DOI: 10.1039/D0NR01740J

nanocomposite materials, which may find broad applications in areas such as coating materials, food packaging, cosmetics, 3D printing and biomedicine.

Acknowledgments

X.Y. and S.C. thank the Donors of the American Chemical Society Petroleum Research Fund for support the simulation part of this research under Grant No. 56884-DNI9. E.O thanks the NASA fellowship from the Iowa Space Grant Consortium (ISGC) for the support of her work. S.J. and E.O. thank the Donors of the American Chemical Society Petroleum Research Fund under Grant No. 60264-DNI7 and funding from the State of Iowa Biosciences Initiative for the experimental part of this research.

References

(1) Arash, B.; Wang, Q.; Varadan, V. K. Mechanical Properties of Carbon Nanotube/Polymer Composites. *Sci. Rep.* **2015**, *4*, 6479.

(2) Coulibaly, S.; Roulin, A.; Balog, S.; Biyani, M. V.; Foster, E. J.; Rowan, S. J.; Fiore, G. L.; Weder, C. Reinforcement of Optically Healable Supramolecular Polymers with Cellulose Nanocrystals. *Macromolecules* **2014**, *47*, 152–160.

(3) Shtein, M.; Nadiv, R.; Buzaglo, M.; Kahil, K.; Regev, O. Thermally Conductive Graphene-Polymer Composites: Size, Percolation, and Synergy Effects. *Chem. Mater.* **2015**, *27*, 2100–2106.

(4) Li, Q.; Chen, L.; Gadinski, M. R.; Zhang, S.; Zhang, G.; Li, H. U.; Iagodkine, E.; Haque, A.; Chen, L.-Q.; Jackson, T. N.; Wang, Q. Flexible High-Temperature Dielectric Materials from Polymer Nanocomposites. *Nature* **2015**, *523*, 576–579.

(5) Ul-Islam, M.; Khattak, W. A.; Ullah, M. W.; Khan, S.; Park, J. K. Synthesis of Regenerated Bacterial Cellulose-Zinc Oxide Nanocomposite Films for Biomedical Applications. *Cellulose* **2014**, *21*, 433–447.

(6) Kumar, S. K.; Benicewicz, B. C.; Vaia, R. A.; Winey, K. I. 50th Anniversary Perspective : Are

View Article Online
DOI: 10.1039/D0NR01740J

Polymer Nanocomposites Practical for Applications? *Macromolecules* **2017**, *50*, 714–731.

(7) Yin, J.; Deng, B. Polymer-Matrix Nanocomposite Membranes for Water Treatment. *J. Memb. Sci.* **2015**, *479*, 256–275.

(8) Chen, G.-G.; Qi, X.-M.; Guan, Y.; Peng, F.; Yao, C.-L.; Sun, R.-C. High Strength Hemicellulose-Based Nanocomposite Film for Food Packaging Applications. *ACS Sustain. Chem. Eng.* **2016**, *4*, 1985–1993.

(9) El Miri, N.; Abdelouahdi, K.; Barakat, A.; Zahouily, M.; Fihri, A.; Solhy, A.; El Achaby, M. Bio-Nanocomposite Films Reinforced with Cellulose Nanocrystals: Rheology of Film-Forming Solutions, Transparency, Water Vapor Barrier and Tensile Properties of Films. *Carbohydr. Polym.* **2015**, *129*, 156–167.

(10) Chatterjee, T.; Krishnamoorti, R. Rheology of Polymer Carbon Nanotubes Composites. *Soft Matter* **2013**, *9*, 9515.

(11) Chen, Q.; Gong, S.; Moll, J.; Zhao, D.; Kumar, S. K.; Colby, R. H. Mechanical Reinforcement of Polymer Nanocomposites from Percolation of a Nanoparticle Network. *ACS Macro Lett.* **2015**, *4*, 398–402.

(12) Kumar, S. K.; Ganesan, V.; Riggleman, R. A. Perspective: Outstanding Theoretical Questions in Polymer-Nanoparticle Hybrids. *J. Chem. Phys.* **2017**, *147*, 020901.

(13) Hooper, J. B.; Schweizer, K. S. Theory of Phase Separation in Polymer Nanocomposites. *Macromolecules* **2006**, *39*, 5133–5142.

(14) Hooper, J. B.; Schweizer, K. S. Contact Aggregation, Bridging, and Steric Stabilization in Dense Polymer−Particle Mixtures. *Macromolecules* **2005**, *38*, 8858–8869.

(15) Mossa, S.; Sciortino, F.; Tartaglia, P.; Zaccarelli, E. Ground-State Clusters for Short-Range Attractive and Long-Range Repulsive Potentials. *Langmuir* **2004**, *20*, 10756–10763.

View Article Online
DOI: 10.1039/D0NR01740J

(16) Pandav, G.; Pryamitsyn, V.; Ganesan, V. Interactions and Aggregation of Charged Nanoparticles in Uncharged Polymer Solutions. *Langmuir* **2015**, *31*, 12328–12338.

(17) Pandav, G.; Pryamitsyn, V.; Errington, J.; Ganesan, V. Multibody Interactions, Phase Behavior, and Clustering in Nanoparticle–Polyelectrolyte Mixtures. *J. Phys. Chem. B* **2015**, *119*, 14536–14550.

(18) Ureña-Benavides, E. E.; Kayatin, M. J.; Davis, V. A. Dispersion and Rheology of Multiwalled Carbon Nanotubes in Unsaturated Polyester Resin. *Macromolecules* **2013**, *46*, 1642–1650.

(19) Hall, L. M.; Schweizer, K. S. Structure, Scattering Patterns and Phase Behavior of Polymer Nanocomposites with Nonspherical Fillers. *Soft Matter* **2010**, *6*, 1015.

(20) Cheng, S.; Carroll, B.; Lu, W.; Fan, F.; Carrillo, J.-M. Y.; Martin, H.; Holt, A. P.; Kang, N.-G.; Bocharova, V.; Mays, J. W.; Sumpter, B. G.; Dadmun, M.; Sokolov, A. P. Interfacial Properties of Polymer Nanocomposites: Role of Chain Rigidity and Dynamic Heterogeneity Length Scale. *Macromolecules* **2017**, *50*, 2397–2406.

(21) Burgos-Mármol, J. J.; Álvarez-Machancoses, Ó.; Patti, A. Modeling the Effect of Polymer Chain Stiffness on the Behavior of Polymer Nanocomposites. *J. Phys. Chem. B* **2017**, *121*, 6245–6256.

(22) Chen, R.; Poling-Skutvik, R.; Howard, M. P.; Nikoubashman, A.; Egorov, S. A.; Conrad, J. C.; Palmer, J. C. Influence of Polymer Flexibility on Nanoparticle Dynamics in Semidilute Solutions. *Soft Matter* **2019**, *15*, 1260–1268.

(23) Olson, E.; Li, Y.; Lin, F.-Y.; Miller, A.; Liu, F.; Tsyrenova, A.; Palm, D.; Curtzwiler, G. W.; Vorst, K. L.; Cochran, E.; Jiang, S. Thin Biobased Transparent UV-Blocking Coating Enabled by Nanoparticle Self-Assembly. *ACS Appl. Mater. Interfaces* **2019**, *11*, 24552–24559.

(24) Khokhlov, A. R.; Semenov, A. N. Liquid-Crystalline Ordering in the Solution of Long Persistent Chains. *Phys. A Stat. Mech. its Appl.* **1981**, *108*, 546–556.

View Article Online
DOI: 10.1039/D0NR01740J

(25) Khokhlov, A. R. Liquid-Crystalline Ordering in the Solution of Semiflexible Macromolecules. *Phys. Lett. A* **1978**, *68*, 135–136.

(26) Kim, J.; Novak, B. M.; Waddon, A. J. Liquid Crystalline Properties of Polyguanidines. *Macromolecules* **2004**, *37*, 8286–8292.

(27) Morozova, S. Methylcellulose Fibrils: A Mini Review. *Polym. Int.* **2020**, *69*, 125–130.

(28) Morozova, S.; Schmidt, P. W.; Metaxas, A.; Bates, F. S.; Lodge, T. P.; Dutcher, C. S. Extensional Flow Behavior of Methylcellulose Solutions Containing Fibrils. *ACS Macro Lett.* **2018**, *7*, 347–352.

(29) De Gennes, P. G. Polymer Solutions near an Interface. Adsorption and Depletion Layers. *Macromolecules* **1981**, *14*, 1637–1644.

(30) Louis, A. A.; Bolhuis, P. G.; Meijer, E. J.; Hansen, J. P. Polymer Induced Depletion Potentials in Polymer-Colloid Mixtures. *J. Chem. Phys.* **2002**, *117*, 1893–1907.

(31) Sankar, U. K.; Tripathy, M. Dispersion, Depletion, and Bridging of Athermal and Attractive Nanorods in Polymer Melt. *Macromolecules* **2015**, *48*, 432–442.

(32) Hall, L. M.; Jayaraman, A.; Schweizer, K. S. Molecular Theories of Polymer Nanocomposites. *Curr. Opin. Solid State Mater. Sci.* **2010**, *14*, 38–48.

(33) Patel, N.; Egorov, S. A. Interactions between Nanocolloidal Particles in Polymer Solutions: Effect of Attractive Interactions. *J. Chem. Phys.* **2005**, *123*, 144916.

(34) Hoogerbrugge, P. J.; Koelman, J. M. V. A. Simulating Microscopic Hydrodynamic Phenomena with Dissipative Particle Dynamics. *Europhys. Lett.* **1992**, *19*, 155–160.

(35) Groot, R. D.; Warren, P. B. Dissipative Particle Dynamics: Bridging the Gap between Atomistic and Mesoscopic Simulation. *J. Chem. Phys.* **1997**, *107*, 4423–4435.

(36) Nikoubashman, A.; Howard, M. P. Equilibrium Dynamics and Shear Rheology of Semiflexible

View Article Online
DOI: 10.1039/D0NR01740J

Polymers in Solution. *Macromolecules* **2017**, *50*, 8279–8289.

(37) Nikoubashman, A.; Milchev, A.; Binder, K. Dynamics of Single Semiflexible Polymers in Dilute Solution. *J. Chem. Phys.* **2016**, *145*, 234903.

(38) Faller, R.; Müller-Plathe, F.; Heuer, A. Local Reorientation Dynamics of Semiflexible Polymers in the Melt. *Macromolecules* **2000**, *33*, 6602–6610.

(39) Nikoubashman, A.; Davis, R. L.; Michal, B. T.; Chaikin, P. M.; Register, R. A.; Panagiotopoulos, A. Z. Thin Films of Homopolymers and Cylinder-Forming Diblock Copolymers under Shear. *ACS Nano* **2014**, *8*, 8015–8026.

(40) Langeloth, M.; Masubuchi, Y.; Böhm, M. C.; Müller-Plathe, F. Recovering the Reptation Dynamics of Polymer Melts in Dissipative Particle Dynamics Simulations via Slip-Springs. *J. Chem. Phys.* **2013**, *138*, 104907.

(41) Ramírez-Hernández, A.; Detcheverry, F. A.; Peters, B. L.; Chappa, V. C.; Schweizer, K. S.; Müller, M.; de Pablo, J. J. Dynamical Simulations of Coarse Grain Polymeric Systems: Rouse and Entangled Dynamics. *Macromolecules* **2013**, *46*, 6287–6299.

(42) Sirk, T. W.; Slizoberg, Y. R.; Brennan, J. K.; Lisal, M.; Andzelm, J. W. An Enhanced Entangled Polymer Model for Dissipative Particle Dynamics. *J. Chem. Phys.* **2012**, *136*, 134903.

(43) Yong, X. Hydrodynamic Interactions and Entanglements of Polymer Solutions in Many-Body Dissipative Particle Dynamics. *Polymers (Basel)*. **2016**, *8*, 426.

(44) Nikunen, P.; Vattulainen, I.; Karttunen, M. Reptational Dynamics in Dissipative Particle Dynamics Simulations of Polymer Melts. *Phys. Rev. E* **2007**, *75*, 036713.

(45) Yong, X.; Kuksenok, O.; Matyjaszewski, K.; Balazs, A. C. Harnessing Interfacially-Active Nanorods to Regenerate Severed Polymer Gels. *Nano Lett.* **2013**, *13*, 6269–6274.

(46) Karatrantos, A.; Clarke, N.; Composto, R. J.; Winey, K. I. Topological Entanglement Length in

View Article Online
DOI: 10.1039/D0NR01740J

Polymer Melts and Nanocomposites by a DPD Polymer Model. *Soft Matter* **2013**, *9*, 3877.

(47) Yong, X. Modeling the Assembly of Polymer-Grafted Nanoparticles at Oil–Water Interfaces. *Langmuir* **2015**, *31*, 11458–11469.

(48) Yong, X.; Qin, S.; Singler, T. J. Nanoparticle-Mediated Evaporation at Liquid–Vapor Interfaces. *Extrem. Mech. Lett.* **2016**, *7*, 90–103.

(49) Chen, S.; Yong, X. Dissipative Particle Dynamics Modeling of Hydrogel Swelling by Osmotic Ensemble Method. *J. Chem. Phys.* **2018**, *149*, 094904.

(50) Chen, S.; Yong, X. Janus Nanoparticles Enable Entropy-Driven Mixing of Bicomponent Hydrogels. *Langmuir* **2019**, *35*, 14840–14848.

(51) Rutledge, G. C. Molecular Simulation of Bundle-like Crystal Nucleation from n -Eicosane Melts. *J. Chem. Phys.* **2011**, *135*, 024903.

(52) Yang, J.-S.; Yang, C.-L.; Wang, M.-S.; Chen, B.-D.; Ma, X.-G. Isothermal Crystallization of Short Polymer Chains Induced by the Oriented Slab and the Stretched Bundle of Polymer: A Molecular Dynamics Simulation. *J. Phys. Chem. B* **2012**, *116*, 2040–2047.

(53) Groot, R. D. Mesoscale Simulation of Semiflexible Chains. II. Evolution Dynamics and Stability of Fiber Bundle Networks. *J. Chem. Phys.* **2013**, *138*, 224904.

(54) Zierenberg, J.; Janke, W. From Amorphous Aggregates to Polymer Bundles: The Role of Stiffness on Structural Phases in Polymer Aggregation. *EPL (Europhysics Lett.* **2015**, *109*, 28002.

(55) Nguyen, L. T.; Yang, W.; Hirst, L. S. Molecular Dynamics Simulation Reveals The Role Of Cross-Linkers In Semi-Flexible Filament Assembly. *Biophys. J.* **2009**, *96*, 126a.

(56) Sheng, Y.-J.; Panagiotopoulos, A. Z.; Kumar, S. K. Effect of Chain Stiffness on Polymer Phase Behavior. *Macromolecules* **1996**, *29*, 4444–4446.

(57) Miller, W. G.; Kou, L.; Tohyama, K.; Voltaggio, V. Kinetic Aspects of the Formation of the

View Article Online
DOI: 10.1039/D0NR01740J

Ordered Phase in Stiff-Chain Helical Polyamino Acids. *J. Polym. Sci. Polym. Symp.* **2007**, *65*, 91–106.

(58) Junghans, C.; Bachmann, M.; Janke, W. Statistical Mechanics of Aggregation and Crystallization for Semiflexible Polymers. *EPL (Europhysics Lett.* **2009**, *87*, 40002.

(59) Kamide, K. *Cellulose and Cellulose Derivatives*; Elsevier, **2005**.

(60) Chen, R.; Poling-Skutvik, R.; Nikoubashman, A.; Howard, M. P.; Conrad, J. C.; Palmer, J. C. Coupling of Nanoparticle Dynamics to Polymer Center-of-Mass Motion in Semidilute Polymer Solutions. *Macromolecules* **2018**, *51*, 1865–1872.

(61) Cai, L.-H.; Panyukov, S.; Rubinstein, M. Mobility of Nonsticky Nanoparticles in Polymer Liquids. *Macromolecules* **2011**, *44*, 7853–7863.

(62) Egorov, S. A. Anomalous Nanoparticle Diffusion in Polymer Solutions and Melts: A Mode-Coupling Theory Study. *J. Chem. Phys.* **2011**, *134*, 084903.

(63) Yamamoto, U.; Schweizer, K. S. Theory of Nanoparticle Diffusion in Unentangled and Entangled Polymer Melts. *J. Chem. Phys.* **2011**, *135*, 224902.

(64) Li, Y.; Chen, S.; Demirci, S.; Qin, S.; Xu, Z.; Olson, E.; Liu, F.; Palm, D.; Yong, X.; Jiang, S. Morphology Evolution of Janus Dumbbell Nanoparticles in Seeded Emulsion Polymerization. *J. Colloid Interface Sci.* **2019**, *543*, 34–42.

(65) Park, S.; Baker, J. O.; Himmel, M. E.; Parilla, P. A.; Johnson, D. K. Cellulose Crystallinity Index: Measurement Techniques and Their Impact on Interpreting Cellulase Performance. *Biotechnol. Biofuels* **2010**, *3*, 10.

(66) Selim, I. Z.; Basta, A. H.; Mansour, O. Y.; Atwa, A. I. Hydroxyethyl Cellulose. II. IR Spectra and Their Relation with the Dielectric Properties of Hydroxyethyl Celluloses. *Polym. Plast. Technol. Eng.* **1994**, *33*, 161–174.

View Article Online
DOI: 10.1039/D0NR01740J

(67) Hu, T.; Yi, J.; Xiao, J.; Zhang, H. Effect of Flexible Spacer Length on the Mesophase Structures of Main-Chain/Side-Chain Liquid Crystalline Polymers Based on Ethyl Cellulose. *Polym. J.* **2010**, *42*, 752–758.

(68) El idrissi, A.; El barkany, S.; Amhamdi, H.; Maaroufi, A.-K. Synthesis and Characterization of the New Cellulose Derivative Films Based on the Hydroxyethyl Cellulose Prepared from Esparto "Stipa Tenacissima" Cellulose of Eastern Morocco. II. Esterification with Acyl Chlorides in a Homogeneous Medium. *J. Appl. Polym. Sci.* **2013**, *127*, 3633–3644.

(69) Brown, W.; Henley, D.; Öhman, J. Studies on Cellulose Derivatives. Part II. The Influence of Solvent and Temperature on the Configuration and Hydrodynamic Behaviour of Hydroxyethyl Cellulose in Dilute Solution. *Die Makromol. Chemie* **1963**, *64*, 49–67.

(70) Banks, W.; Greenwood, C. T. The Conformation of Amylose in Neutral, Aqueous Salt Solution. *Carbohydr. Res.* **1968**, *7*, 349–356.

(71) Genix, A. C.; Oberdisse, J. Nanoparticle Self-Assembly: From Interactions in Suspension to Polymer Nanocomposites. *Soft Matter*, **2018**, *14*, 5161–5179.

(72) Karatrantos, A.; Koutsawa, Y.; Dubois, P.; Clarke, N.; Kröger, M. Miscibility and Nanoparticle Diffusion in Ionic Nanocomposites. *Polymers (Basel).* **2018**, *10*, 1010.

(73) González-Melchor, M.; Mayoral, E.; Velázquez, M. E.; Alejandre, J. J.; González-Melchor, M.; Mayoral, E.; Velázquez, M. E.; Alejandre, J. J. Electrostatic Interactions in Dissipative Particle Dynamics Using the Ewald Sums. *J. Chem. Phys.* **2006**, *125*, 224107.

(74) Qin, S.; Kang, J.; Yong, X. Structure and Dynamics of Stimuli-Responsive Nanoparticle Monolayers at Fluid Interfaces. *Langmuir* **2018**, *34*, 5581–5591.

(75) Qin, S.; Yong, X. Interfacial Adsorption of PH-Responsive Polymers and Nanoparticles. *Soft Matter* **2017**, *13*, 5137–5149.

View Article Online
DOI: 10.1039/D0NR01740J

(76) Groot, R. D. Electrostatic Interactions in Dissipative Particle Dynamics—Simulation of Polyelectrolytes and Anionic Surfactants. *J. Chem. Phys.* **2003**, *118*, 11265–11277.

(77) O'Neal, J. T.; Bolen, M. J.; Dai, E. Y.; Lutkenhaus, J. L. Hydrogen-Bonded Polymer Nanocomposites Containing Discrete Layers of Gold Nanoparticles. *J. Colloid Interface Sci.* **2017**, *485*, 260–268.

(78) Heo, K.; Miesch, C.; Emrick, T.; Hayward, R. C. Thermally Reversible Aggregation of Gold Nanoparticles in Polymer Nanocomposites through Hydrogen Bonding. *Nano Lett.* **2013**, *13*, 5297–5302.

(79) Cheng, S.; Xie, S.-J.; Carrillo, J.-M. Y.; Carroll, B.; Martin, H.; Cao, P.-F.; Dadmun, M. D.; Sumpter, B. G.; Novikov, V. N.; Schweizer, K. S.; Sokolov, A. P. Big Effect of Small Nanoparticles: A Shift in Paradigm for Polymer Nanocomposites. *ACS Nano* **2017**, *11*, 752–759.

(80) Emamy, H.; Kumar, S. K.; Starr, F. W. Diminishing Interfacial Effects with Decreasing Nanoparticle Size in Polymer-Nanoparticle Composites. *Phys. Rev. Lett.* **2018**, *121*, 207801.

(81) Starr, F. W.; Douglas, J. F.; Meng, D.; Kumar, S. K. Bound Layers "Cloak" Nanoparticles in Strongly Interacting Polymer Nanocomposites. *ACS Nano* **2016**, *10*, 10960–10965.

View Article Online
DOI: 10.1039/D0NR01740J

Table of Contents

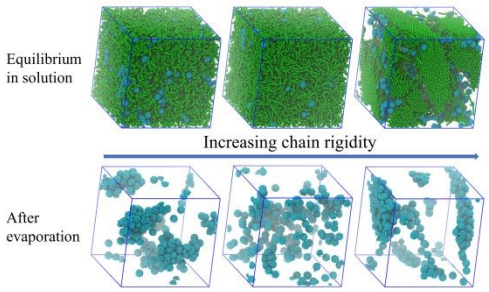

Nanoparticle aggregation in a nanocomposite can be physically modulated by the polymer conformational change into open fractal structures.